

Surface-activated direct bonding of diamond (100) and *c*-plane sapphire with high transparency for quantum applications

To cite this article: Tetsuya Miyatake *et al* 2023 *Jpn. J. Appl. Phys.* **62** 096503


View the [article online](#) for updates and enhancements.

You may also like

- [Overview of recent direct wafer bonding advances and applications](#)
H Moriceau, F Rieutord, F Fournel et al.
- [Water Stress Corrosion in Bonded Structures](#)
F. Fournel, C. Martin-Cocher, D. Radisson et al.
- [Investigation of Plasma Activation Directions for Low-Damage Direct Bonding](#)
Shicheng Zhou, Xiaoyun Qi, Hui Fang et al.



Surface-activated direct bonding of diamond (100) and *c*-plane sapphire with high transparency for quantum applications

Tetsuya Miyatake^{1*}, Kenichi Kawaguchi^{1*}, Manabu Ohtomo¹ , Toshiki Iwai¹, Tetsuro Ishiguro¹, Yoshiyasu Doi¹, Jeffrel Hermias², Salahuddin Nur², Ryoichi Ishihara², and Shintaro Sato¹

¹Quantum Hardware Core Project, Quantum Laboratory, Fujitsu Research, Fujitsu Limited, 10-1 Morinosato-Wakamiya, Atsugi, Kanagawa, 243-0197, Japan

²QuTech, Delft University of Technology, Mekelweg 4, 2628CD Delft, The Netherlands

*E-mail: miyatake.tetsuya@fujitsu.com; k_kawaguchi@fujitsu.com

Received April 10, 2023; revised August 24, 2023; accepted August 24, 2023; published online September 27, 2023

Surface-activated direct bonding of diamond (100) and *c*-plane sapphire substrates is investigated using Ar atom beam irradiation and high-pressure contact at RT. The success probability of bonding strongly depends on the surface properties, i.e., atomic smoothness for the micron-order area and global flatness for the entire substrate. Structural analysis reveals that transformation from sapphire to Al-rich amorphous layer is key to obtaining stable bonding. The beam irradiation time has optimal conditions for sufficiently strong bonding, and strong bonding with a shear strength of more than 14 MPa is successfully realized. Moreover, by evaluating the photoluminescence of nitrogen-vacancy centers in the diamond substrate, the bonding interface is confirmed to have high transparency in the visible wavelength region. These results indicate that the method used in this work is a promising fabrication platform for quantum modules using diamonds. © 2023 The Japan Society of Applied Physics

1. Introduction

Diamonds are wide bandgap semiconductor materials with high breakdown voltage and excellent heat conduction, and have been used in power electronics. More recently, diamonds have attracted attention for quantum applications because they allow the formation of color centers with stable spins. Diamonds with color centers are applied to quantum sensors, quantum communications, and quantum computers. The light emission from a color center in a diamond spin qubit is used as the readout and/or control of quantum information. Coupling the emitted light from color centers to photonic circuits integrated with functionalized components is necessary to read out and/or control quantum information. Single-crystal diamond substrates with high purity grown using CVD are used for quantum device applications. However, the substrate size is currently limited to 1 inch^{1,2)} because of the technological challenges in the formation of large seed crystals and the CVD of diamonds. Therefore, diamond substrates must be bonded to other larger wafers to fabricate a large-scale quantum photonic circuit from the spins in diamonds. Photonic circuits are fabricated on the larger wafer side of heterogeneously integrated wafers.³⁾ The luminescence of color centers is in the visible wavelength region of approximately 600 nm. Bonding diamonds with a transparent material with low optical loss in the visible wavelength region is required to access the quantum states of color centers using an optical technique. Sapphires are promising candidates as transparent materials because they are single crystals with large optical bandgaps.⁴⁾

Si has been used as a mother substrate in the wafer bonding of diamonds because it is a common semiconductor wafer for electronics. In addition to bare silicon,^{5–7)} Si covered with SiO₂^{8,9)} has been used. In previous studies, wet process-based bonding was used with chemical treatments. In Ref. 6, a diamond substrate with the (100) surface was compared with that of the (111) surface. In wet process-based bonding, it is difficult for diamond (100) to bond because it cannot be terminated with the hydroxyl groups that constitute the bonding interface. This implies the difficulty of applying wet

bonding to diamonds (100). Alternatively, dry process-based bonding is a possible choice for bonding diamond (100) to mother substrates. Atomic diffusion bonding (ADB)^{10–17)} and surface activation bonding (SAB)^{7,18–32)} have been reported for various material combinations. ADB is a promising technique for some applications and can ensure chemical bond formation by atom diffusion. For quantum applications, however, the influence of diffusion of bonding elements into diamonds is currently unclear. Instead, SAB can be a good candidate for this purpose, because it directly bonds two wafers without using any additional materials.

In this study, we investigate the direct bonding of diamond (100) substrates with *c*-plane sapphire wafers for quantum applications using SAB. We reveal the required properties of the diamond surface for bonding. We show that the diamond (100) and *c*-plane sapphire substrates are successfully bonded with a shear strength of more than 14 MPa. Moreover, we characterize the bonding interface and discuss the possible bonding mechanisms.

2. Experimental methods

Diamond (100) and sapphire (1000) substrates are used for the experiments. The single-crystal diamond substrate is heteroepitaxially grown using CVD and contains approximately 3 ppm of nitrogen impurities. The size and thickness of the diamond are 4 mm × 4 mm and 0.5 mm, respectively. The diameter of a sapphire wafer is 4 inches. SAB is performed using a machine manufactured by Nidec Machine Tool Corporation (BOND MEISTER MWB-08/12-ST) and includes the following procedures: first, the substrates are cleaned with an alkaline solution to remove organic contaminants and residual particles. Then, irradiation with an Ar fast atom beam (FAB) in a vacuum chamber removes an inert layer (oxide film or deposit) on the surface to be bonded and form dangling bonds on the surface. The FAB source is a neutralized atom beam generated with a voltage of 1.8 kV and a current of 100 mA. The background vacuum condition during the surface activation process is maintained at less than 1.0×10^{-5} Pa. The surfaces of both substrates are simultaneously irradiated with FAB. Then the

activated surfaces are brought into contact with each other and a pressure of 20 MPa is applied.

The surface properties are investigated using atomic force microscopy (AFM) and coherence scanning interferometry (CSI). The characteristic change of diamond surface by FAB irradiation is investigated using Raman spectroscopy and X-ray photoelectron spectroscopy (XPS). Structural characterization of the bonding interface is performed using transmission electron microscopy (TEM) and energy dispersive X-ray spectroscopy (EDX). The bonding strength is measured through a shear strength test suitable for evaluating bonded substrates in which chips with large size differences are bonded together.

3. Results and discussion

3.1. Influence of the surface properties of the diamond substrate

In contrast to well-established semiconductor wafers, such as Si, commercially available diamond substrates have larger variations in surface properties because polishing technologies remain immature due to the hardness of diamonds. Diamond surfaces often have a roughness of more than 0.5 nm for a $10\ \mu\text{m} \times 10\ \mu\text{m}$ area and an unevenness of more than 500 nm over the chip. Therefore, we first investigate the influence of surface properties of diamond substrates on the probability of bonding success. We prepare diamond substrates with varying surface properties from various manufacturers. Some diamond substrates are subjected to additional polishing using the lapping or chemical mechanical polishing,^{33–35} to increase the number of diamond substrates with flat and smooth surfaces.

Figure 1 shows the bonding results for diamonds with various surfaces and sapphires. The bonding conditions other than FAB irradiation time are the same for all samples. The FAB irradiation time is 90 s or more. We use two metrics: the overall flatness of the substrate and the surface roughness (arithmetic mean roughness) for an area of $10\ \mu\text{m} \times 10\ \mu\text{m}$. The overall flatness and micro-area roughness are evaluated using CSI and AFM, respectively. The surface roughness was measured before FAB irradiation. The substrates with a surface roughness of less than 0.2 nm are prepared by applying a precise polishing procedure; however, those

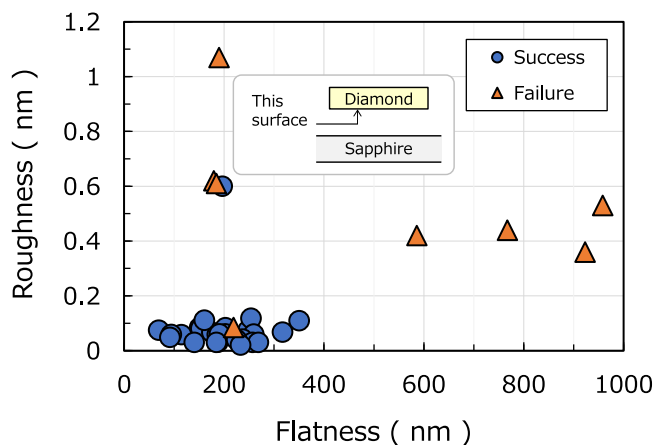


Fig. 1. Surface properties of diamond substrates for bonding. The measurement surface is the bonding surface of the diamond (see insert). A circle indicates successful bonding, whereas a triangle indicates failed bonding.

with a surface roughness of more than 0.5 nm are not subjected to this procedure. The surface roughness of sapphire is less than 0.3 nm. In Fig. 1, the circular symbol indicates successful bonding, whereas the triangular symbol indicates failed bonding. The results clearly show that a well-controlled diamond surface is necessary for bonding. Bonding requires a roughness of less than 0.2 nm and an unevenness of less than 300 nm.^{36,37} Figure 2 shows an example of the AFM and CSI profiles for the diamond used in successful bonding. The surface roughness and flatness are small, and it is smooth and has little unevenness. FAB irradiation does not change the overall flatness of the diamond because its etching amount is negligible. In subsequent sections, we discuss the details of the nanoscale surface modulation introduced by FAB irradiation.

3.2. Bonding interface of diamond (100)/sapphire (1000)

The bonding interface is investigated using cross-sectional TEM. The specimen for this study is fabricated using laser cutting because of the hardness of the diamond and sapphire substrates. Figure 3(a) shows a cross-sectional TEM image with low magnification. The FAB irradiation time is 270 s. An intermediate layer of approximately 300 nm thickness is formed between the diamond and sapphire substrates. In Fig. 3(a), a relatively large scratch of approximately 35 nm in width and 20 nm in depth is observed on the diamond bottom surface near the center of the TEM image. This scratch is left after polishing and is not generated during the bonding process or TEM observation sample preparation. In the current diamond polishing technology, some possibilities exist that deep scratches remain even after polishing. However, the number of scratches can be reduced sufficiently so that bonding is least affected. Under low magnification, the interface between the diamond and the intermediate layer is relatively smooth, whereas that between the sapphire and

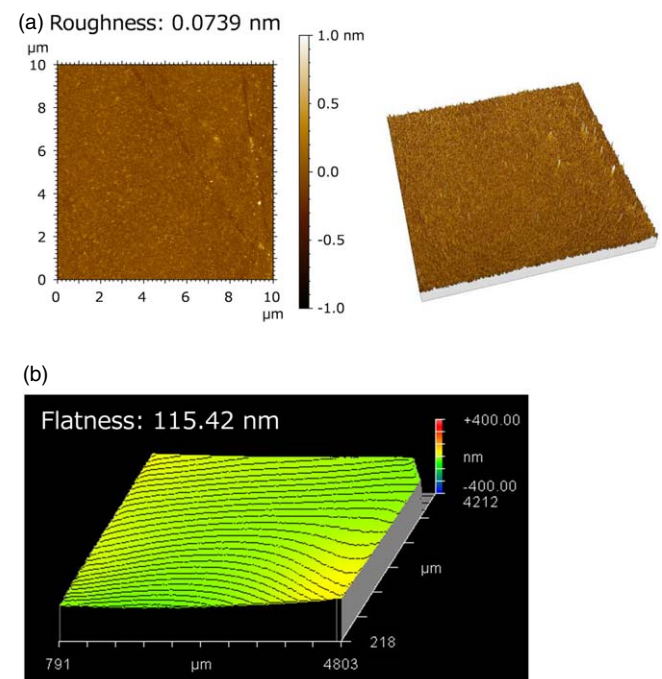


Fig. 2. Examples of measurement results of surface roughness (a) and flatness (b). The surface of the diamond substrate, which is successfully bonded, is smooth without minute unevenness and is flat.

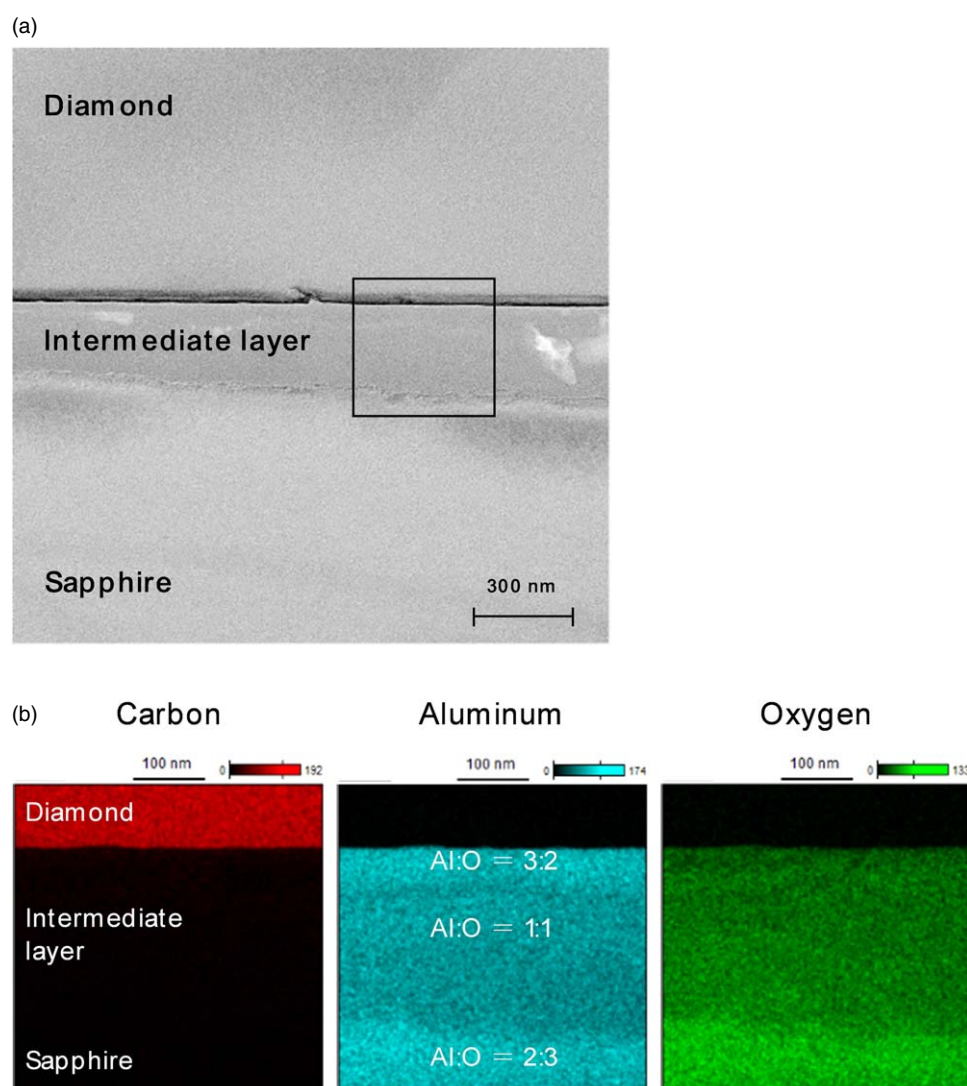


Fig. 3. Cross-sectional TEM image of the bonding interface (a) and the EDX spectroscopy measurement results of the interlayer (b). An intermediate layer with a thickness of approximately 300 nm was observed at the junction interface between the diamond and sapphire substrates. Al and O are detected in the interlayer, whereas carbon is not detected.

the intermediate layer is not. The thickness of the intermediate layer formed by FAB irradiation has some variations, and the undulated interface of the intermediate layer and sapphire crystal is defined by its variations. Figure 3(b) shows the results of the elemental mapping obtained via the EDX of the bonding interface including the interlayer. The interlayer is confirmed to be composed of Al and O only, indicating that the intermediate layer is formed by the alteration of sapphire (Al_2O_3) through FAB irradiation. Additionally, this result implies that the irradiated Ar atoms barely penetrate the inside of the diamond crystal and instead penetrate the inside of the sapphire crystal to a depth of a few hundred nanometers. Although the Al and O composition ratio of sapphire is 2:3, that of the intermediate layer is 1:1 at the center of the layer and 3:2 near the interface of the diamond substrate. The ratio of O to Al decreases as the diamond surface approaches because O is removed from the sapphire during the formation of the intermediate layer by FAB irradiation. Regarding the effect of Ar irradiation on sapphire, Ar ion sputtering has been investigated with various metal oxides.³⁸⁾ X-ray photoelectron spectrum analysis shows that Ar ions can induce the disorder of sapphire

bond angles. A similar effect is considered to occur in this work, although neutralized atoms are used.

During diamond processing, diamond surface carbonization is often observed.^{39–41)} Therefore, the surface of the FAB-irradiated diamond is investigated using Raman spectrum measurement, which provides sufficient sensitivity for detecting the formation of monolayer-thick graphene. The Raman spectrum of the surface of the diamond substrate subjected to FAB irradiation for 270 s is shown in Fig. 4(a). Raman spectrum for graphite is also provided as a reference. Raman measurement is performed using a 488 nm wavelength laser on the reflection configuration. In Fig. 4(a), no peaks due to graphite are observed in the FAB-irradiated diamond. In order to evaluate the carbonization by FAB irradiation in more detail, we measure the XPS (Al $K\alpha$ X-ray source) of the diamond substrate irradiated by FAB. The measurement results are shown in Fig. 4(b). The binding energy is shifted due to the charging effect. From these results, it is found that the sp^2 peak increased with FAB irradiation. The energy difference between sp^3 and sp^2 is 1.0 eV, which is almost consistent with the previous research.⁷⁾ The value of $\text{sp}^2/(\text{sp}^2 + \text{sp}^3)$ calculated from the

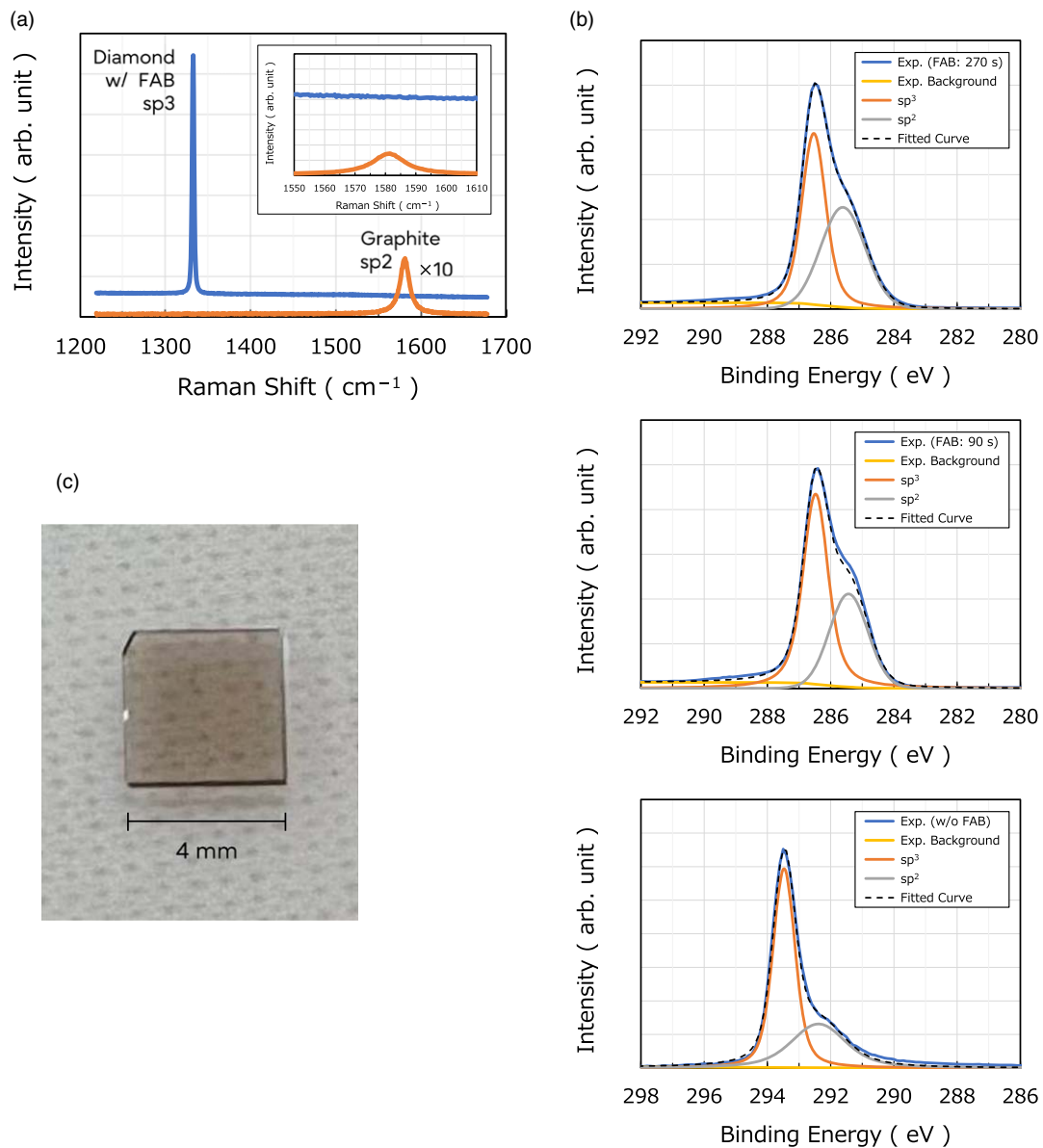


Fig. 4. (a) Raman spectrum of the diamond substrate irradiated with FAB for 270 s. No peaks due to graphite are observed in the FAB-irradiated diamond. (b) C 1s photoemission spectra of diamond substrates without and with FAB irradiation. The sp^2 peak increased with FAB irradiation. (c) An image of the bonding of the diamond and sapphire substrates. The color of the diamond is the original color due to impurities and not due to the bonding interface.

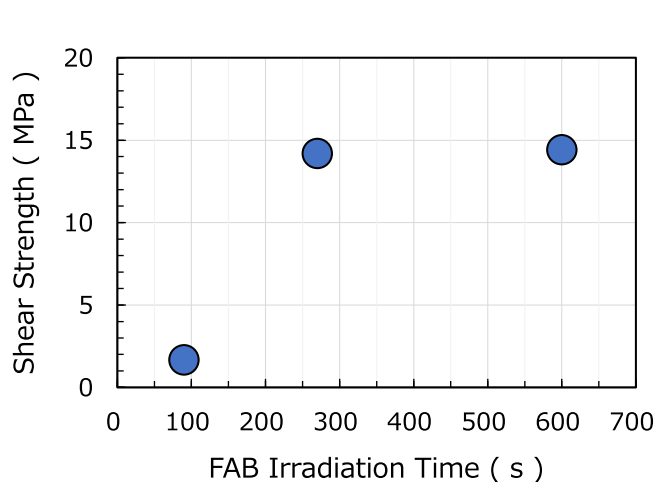


Fig. 5. Relationship between FAB irradiation time and shear strength. The shear strength is almost the same and exceeds 14 MPa after 270 s and 600 s of FAB irradiation; however, it has a very low value of 2 MPa after 90 s of FAB irradiation.

areas of sp^2 and sp^3 peaks increases from 35.4% to 38.2% by 90 s of FAB irradiation. This suggests that a few parts of the diamond crystals decompose into amorphous carbon or graphite. At 270 s of FAB irradiation, sp^2 increases and the $sp^2/(sp^2 + sp^3)$ ratio increases to 47.9%. The decomposition to amorphous carbon or graphite increases with increasing FAB irradiation time. However, even after the long irradiation time, the sp^2 peak is not dominant. This result differs from previous studies,³²⁾ but we speculate that this may be associated with a difference in crystallinity. From Raman and XPS results, it is considered that the carbonization by FAB irradiation is not uniformly formed on the surface of the diamond substrate, but a small carbonization region is partially formed. Figure 4(c) shows a photograph of the bonded sample. No interference fringes are observed on the bonding surface, indicating that the entire surface of the diamond substrate is bonded to the sapphire substrate. The color of the diamond does not originate from the bonding interface but from the diamond crystal itself, because this

CVD diamond contains N impurities with a concentration of approximately 3 ppm.

3.3. Effect of bonding conditions

We investigate the bonding strength of the bonded substrates by changing the FAB irradiation conditions. It is evaluated using shear strength. Figure 5 shows the relation between FAB irradiation time and shear strength. The shear strengths of the samples bonded with FAB irradiation times of 270 and 600 s are 14.19 and 14.41 MPa, respectively. In the substrate bonded under the condition of shear strength greater than 14 MPa, delamination occurs between the diamond and the intermediate layer, or between sapphire and the intermediate layer. Therefore, some intermediate layer pieces are observed on the diamond surface after delamination. Although the shear test was performed once per FAB condition, the results imply that the mechanical strength of both interfaces is similar. In contrast, the sample bonded with a FAB irradiation time of 90 s shows considerably small shear strength of 2 MPa. For this sample, peeling occurred at the interface between the diamond substrate and the intermediate layer, which is consistent with the fact that the bonding interface is weak for that bonding condition. This result indicates that a specific duration of FAB irradiation is necessary to achieve sufficient bonding strength. Compared with the result of 1.7 MPa for diamond (100)/Si obtained through the wet method,⁵⁾ our result of 14 MPa is sufficiently large. The shear strength of approximately 14 MPa is comparable with the reported values for bonding of the same material. The bonding strength of SAB in the same material is 25 MPa or more for SiO₂/SiO₂,¹⁹⁾ 6.47 MPa or more for Cu/Cu,²²⁾ and 14 MPa or more for Ge/Ge.²⁴⁾ These bonding strengths are extracted from the tensile test, not the shear test.

Figure 6 shows the TEM images of the bonding interface for various FAB irradiation times. When the FAB irradiation times are 600 s and 270 s, the intermediate layer has a thickness of 200–300 nm. However, when the FAB irradiation time is 90 s, the thickness of the intermediate layer is 10 nm.⁴²⁾ This result indicates that the formation speed of the amorphous layer is nonlinear to the FAB irradiation time. Such a nonlinear formation process of intermediate layers induces a large difference in the shear strength results. For the bonding of diamond and sapphire, a thick amorphous layer is necessary to obtain strong bonding strength. The Al content of the c intermediate layer increases with increasing FAB irradiation time. In the case of FAB irradiation for 270 s, the composition ratio of Al to O is 3:2 near the bonding interface and 1:1 in the middle of the intermediate layer, as described above. In the case of FAB irradiation for 600 s, the composition ratio of Al and O is 2:1 near the bonding interface and 5:4 in the middle of the intermediate layer. This result implies that O desorption occurs continuously during FAB irradiation.

Figure 7 shows high-magnification TEM images of the interface between the diamond and the intermediate layer. First, the interfaces of the diamond and the intermediate layer of the 90 s sample and the other samples have different shapes. The 90 s sample has a relatively flat interface, while the other samples have undulating interfaces. The sample preparation for TEM observation is carefully performed; therefore, this TEM image is considered to show the original bonding interface. As discussed above, the

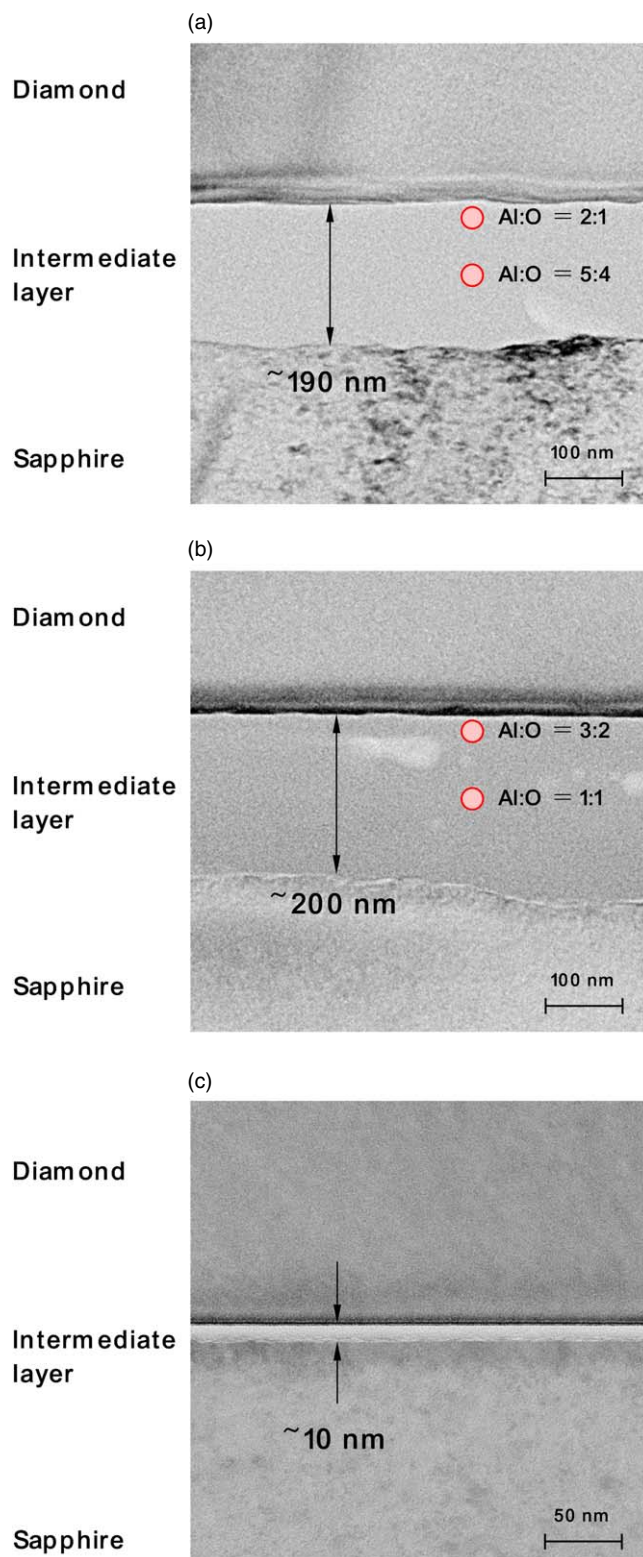


Fig. 6. TEM images of the bonding interface at various FAB irradiation time slots. Under FAB irradiation for (a) 600 s and (b) 270 s, approximately 200 nm intermediate layer is observed. The composition ratio of Al and O in the intermediate layer differs between FAB irradiation for 600 s and 270 s, and the composition ratio of O is smaller under FAB irradiation for 600 s. Under FAB irradiation for 90 s shown in (c), the intermediate layer has thickness of only 10 nm.

existence of elements C, Al, and O has abruptly changed at the interfaces. The undulation of the interfaces is defined by the diamond surface. This means that FAB irradiation modified the diamond bottom surface. We evaluate the

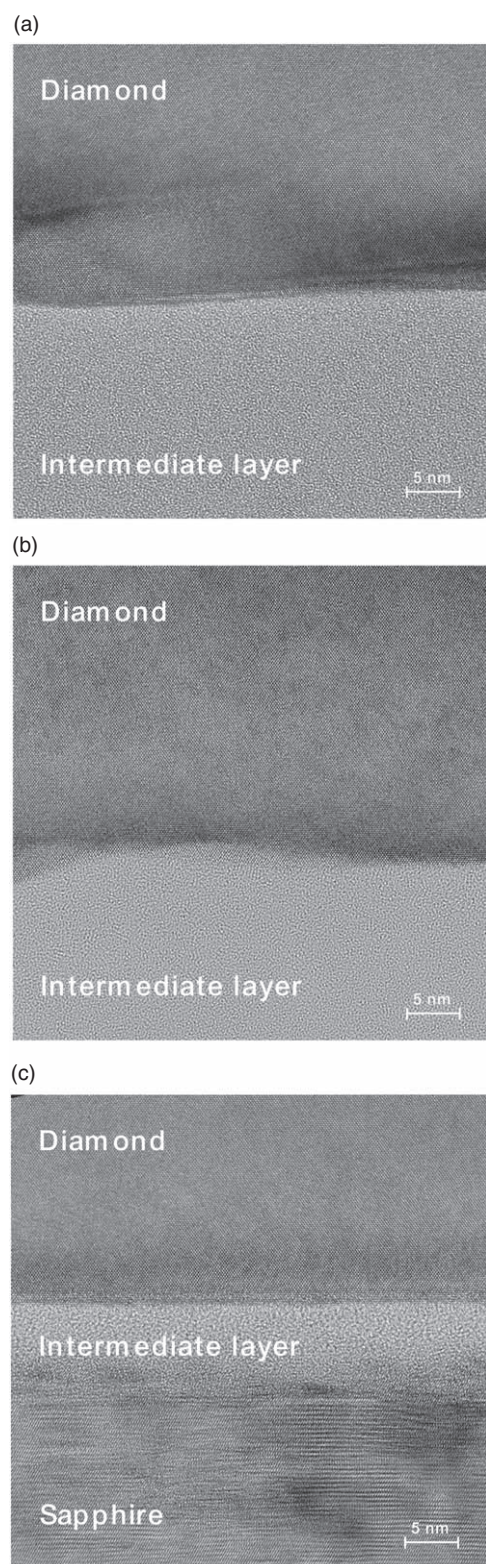


Fig. 7. High magnification TEM images of the interface. Under FAB irradiation for (a) 600 s and (b) 270 s, the interface between the diamond and the intermediate layer is slightly undulated. Under FAB irradiation for 90 s (c), the interface between the diamond and the intermediate layer is flat.

diamond etching rate of FAB irradiation using reference diamonds with longer FAB irradiation times. The etching rate is approximately 0.09 nm min^{-1} , indicating that the etching amount of the diamond is approximately 1 nm even at an irradiation time of 600 s. Thus, FAB irradiation is considered only to affect the undulation formation on the

diamond bottom surface by *local etching*. The interfaces touch each other completely, illustrating that the intermediate layer is deformed to fit the undulating diamond surface. The crystallinity of the intermediate layer is clarified based on TEM observations aligned to the (10–10) and (11–20) directions of the sapphire. No crystal structure is observed in the intermediate layer. Therefore, the intermediate layer is amorphous. Consistent with the fact that the intermediate layer deforms to fit the undulating diamond surface, the amorphous layer is generally softer than the crystal. In the TEM images, some dark contrasting regions are observed at the interfaces, implying the existence of local strain. Under the conditions of this experiment, FAB irradiation has a different effect on the diamond and sapphire crystals. FAB irradiation etches only approximately 1 nm without changing the crystallinity of the diamonds; however, it causes the sapphire crystals to change from single crystals into amorphous crystals. As can be inferred from the EDX results in Fig. 3 and the magnified TEM image in Fig. 7, the interdiffusion of diamond and sapphire at the bonding interface is negligible.

Here, we discuss the mechanism of this bonding technique. FAB irradiation modifies the sapphire surface, forming an amorphous AlO_x layer. The amorphous AlO_x layer has numerous dangling bonds in various directions. Therefore, the surface atoms of the diamond can easily find their counterpart bonds, resulting in strong bonding between diamond and sapphire. In this experiment, the FAB irradiation time for the diamond surface is changed at the same time, which also affected the increase in the dangling bonds on the diamond side. In particular, the formation of the nanoscale undulating surface of the diamond might provide dangling bonds with various angles. Given that the surface of the interlayer contains Al-rich AlO_x , the expected dominant chemical bond is C–Al. Clarification of the chemical bond is beyond this study. Not only the number of chemically active bonds but also the elastic properties of the intermediate AlO_x layer contribute to the bonding process. Given that the amorphous AlO_x layer is softer than the sapphire crystal, the intermediate layer deforms and contacts perfectly with the diamond surface with nanoscale roughness when the diamond and sapphire are pressed under a pressure of 20 MPa. This phenomenon might increase the adhesion between diamond and sapphire substrates. Strong bonding to diamond (100) is realized under these effects.

3.4. Optical properties of bonded substrates

We measure the photoluminescence (PL) of the natural nitrogen-vacancy (NV) center in the diamond substrate to evaluate the transparency of the bonding interface of the diamond (100)/c-plane sapphire sample. Two measurement configurations for the same sample are used to evaluate the transparency of the bonded interface, as shown in Figs. 8(a) and 8(b). In the Fig. 8(a) configuration, the excitation laser is illuminated on the bonded substrate from the sapphire side and the PL of the NV centers is detected by transmitting through the bonded interface. In the Fig. 8(b) configuration, the PL of the NV centers is measured directly from the diamond surface side. Figure 8(c) shows the PL spectra obtained at RT. Peaks at 637 nm correspond to the zero-phonon emission wavelength of the NV centers in the

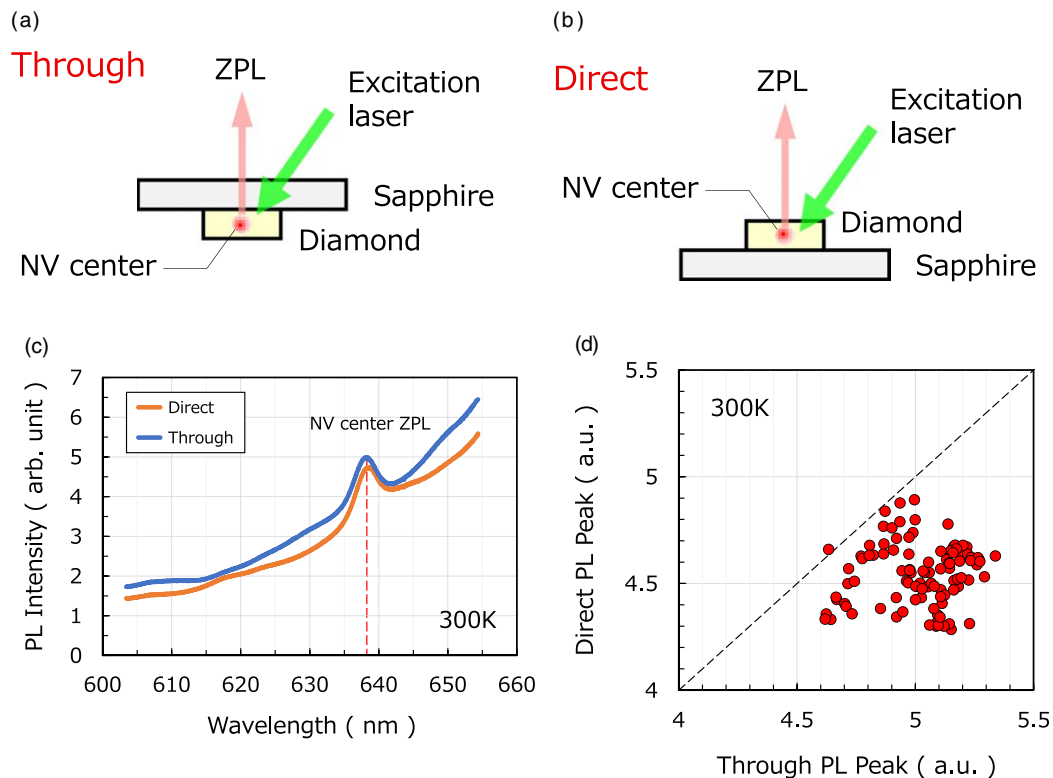


Fig. 8. (a), (b) Two measurement configurations for the same sample used to evaluate the transparency of the bonded interface. (c) The PL spectra of the NV centers obtained with two configurations. The peaks at 637 nm correspond to the zero-phonon emission wavelength of the NV center of diamond. (d) Correlation of peak intensities measured by both configurations in 100 measurement points.

diamond. In Fig. 8(c), it can be seen that the intensity of the PL peaks transmitted through the bonding interface is stronger than that of the PL peaks measured directly. It is considered that this is because the PL extraction efficiency is improved when the PL is excited from the sapphire side due to the difference in refractive index between air and sapphire. Furthermore, in order to increase the reliability of the measured data, we measured PL at 100 different points on one bonded substrate. Figure 8(d) shows the correlation of peak intensities measured for both configurations in 100 measurement points. It is confirmed that the PL peak intensity in the case of excitation from the sapphire side is stronger than that in the case of excitation from the diamond side at almost all measurement points. Since PL measurements are uniform, it is considered that our bonding interface has good homogeneity. This result indicates that the transmittance of the bonding interface of the substrate bonded by the SAB is sufficiently high.

4. Conclusions

This study conducted RT direct bonding using surface-activated bonding of diamond and sapphire substrates. This bonding method is a fundamental technology for manufacturing quantum chips with small diamond substrates. Successful bonding is demonstrated, which clarifies the requirements for the diamond surface. The diamond surface must have a roughness of <0.2 nm and unevenness of <300 nm. The amorphous AlO_x layer formed during FAB irradiation enables perfect bonding, and the possible mechanism is discussed. The sufficient bonding strength of 14.41 MPa is confirmed by measuring the shear strength of the bonded substrate, and the high transparency of the bonding interface is demonstrated by the PL from the NV

centers in the diamond substrate. The results of this work are promising for the fabrication of integrated quantum chips using diamond color centers.

Acknowledgments

The authors would like to thank D-process Inc. for their cooperation in the substrate bonding process. The authors would like to thank N. Fushimi in Fujitsu Limited for providing technical assistance.

ORCID iDs

Manabu Ohtomo  <https://orcid.org/0000-0001-8361-956X>

- 1) Y. Mokuno, A. Chayahara, and H. Yamada, *Diam. Relat. Mater.* **17**, 415 (2008).
- 2) S.-W. Kim, Y. Kawamata, R. Takaya, K. Koyama, and M. Kasu, *Appl. Phys. Lett.* **117**, 202102 (2020).
- 3) R. Ishihara et al., 2021 IEEE Int. Electron Devices Meeting (IEDM), p. 14.5.
- 4) E. T. Arakawa and M. W. Williams, *J. Phys. Chem. Solids* **29**, 735 (1968).
- 5) T. Matsumae, Y. Kurashima, H. Takagi, H. Umezawa, and E. Higurashi, *Scr. Mater.* **191**, 52 (2021).
- 6) T. Matsumae, Y. Kurashima, H. Umezawa, and H. Takagi, *Scr. Mater.* **175**, 24 (2020).
- 7) J. Liang, S. Masuya, M. Kasu, and N. Shigekawa, *Appl. Phys. Lett.* **110**, 111603 (2017).
- 8) S. Fukumoto, T. Matsumae, Y. Kurashima, H. Takagi, H. Umezawa, M. Hayase, and E. Higurashi, *Appl. Phys. Lett.* **117**, 201601 (2020).
- 9) T. Matsumae, Y. Kurashima, H. Umezawa, and H. Takagi, *Jpn. J. Appl. Phys.* **59**, SBBA01 (2020).
- 10) T. Amino, M. Uomoto, and T. Shimatsu, *ECS J. Solid State Sci. Technol.* **10**, 054008 (2021).
- 11) T. Shimatsu and M. Uomoto, *ECS Trans.* **33**, 61 (2010).
- 12) T. Shimatsu, M. Uomoto, and H. Kon, *ECS Trans.* **64**, 317 (2014).
- 13) G. Yonezawa, Y. Takahashi, Y. Sato, S. Abe, M. Uomoto, and T. Shimatsu, *ECS Trans.* **86**, 233 (2018).

- 14) G. Yonezawa, Y. Takahashi, Y. Sato, S. Abe, M. Uomoto, and T. Shimatsu, *Jpn. J. Appl. Phys.* **59**, SBBC03 (2020).
- 15) M. Uomoto and T. Shimatsu, *Jpn. J. Appl. Phys.* **59**, SBBC04 (2020).
- 16) T. Amino, M. Uomoto, and T. Shimatsu, *Jpn. J. Appl. Phys.* **61**, SF1002 (2022).
- 17) T. Matsumae, Y. Kurashima, H. Umezawa, Y. Mokuno, and H. Takagi, *Microelectron. Eng.* **195**, 68 (2018).
- 18) H. Takagi, K. Kikuchi, R. Maeda, T. R. Chung, and T. Suga, *Appl. Phys. Lett.* **68**, 2222 (1996).
- 19) J. Utsumi, K. Ide, and Y. Ichiyanagi, *Jpn. J. Appl. Phys.* **55**, 026503 (2016).
- 20) J. Liang, Y. Zhou, S. Masuya, F. Guemann, M. Singh, J. Pomeroy, S. Kim, M. Kuball, M. Kasu, and N. Shigekawa, *Diam. Relat. Mater.* **93**, 187 (2019).
- 21) M. M. R. Howlader, T. Suga, F. Zhang, T. H. Lee, and M. J. Kim, *Electrochem. Solid-State Lett.* **13**, H61 (2010).
- 22) T. H. Kim, M. M. R. Howlader, T. Itoh, and T. Suga, *J. Vac. Sci. Technol. A* **21**, 449 (2003).
- 23) H. Takagi, R. Maeda, N. Hosoda, and T. Suga, *Jpn. J. Appl. Phys.* **38**, 1589 (1999).
- 24) E. Higurashi, Y. Sasaki, R. Kurayama, T. Suga, Y. Doi, Y. Sawayama, and I. Hosako, *Jpn. J. Appl. Phys.* **54**, 030213 (2015).
- 25) J. Utsumi, K. Ide, and Y. Ichiyanagi, *Micro Nano Eng.* **2**, 1 (2019).
- 26) J. Utsumi, K. Ide, and Y. Ichiyanagi, *ECS Trans.* **75**, 355 (2016).
- 27) S. Kanda, Y. Shimizu, Y. Ohno, K. Shirasaki, Y. Nagai, M. Kasu, N. Shigekawa, and J. Liang, *Jpn. J. Appl. Phys.* **59**, SBBC03 (2020).
- 28) Y. Ohno, J. Liang, H. Yoshida, Y. Shimizu, Y. Nagai, and N. Shigekawa, *Jpn. J. Appl. Phys.* **61**, SF1006 (2022).
- 29) Y. Kurashima, A. Maeda, and H. Takagi, *Microelectron. Eng.* **118**, 1 (2014).
- 30) J. Utsumi and R. Takigawa, *Scr. Mater.* **191**, 215 (2021).
- 31) J. Liang, S. Yamajo, M. Kuball, and N. Shigekawa, *Scr. Mater.* **159**, 58 (2019).
- 32) M. Fujino, N. Hosoda, T. Suga, N. Ishikawa, and N. Kuwayama, *Jpn. J. Appl. Phys.* **54**, 081301 (2015).
- 33) A. Kubota, S. Fukuyama, Y. Ichimori, and M. Touge, *Diam. Relat. Mater.* **24**, 59 (2012).
- 34) A. Kubota, S. Nagae, S. Motoyama, and M. Touge, *Diam. Relat. Mater.* **60**, 75 (2015).
- 35) E. L. H. Thomas, S. Mandal, E. B. Brousseau, and O. A. Williams, *Sci. Technol. Adv. Mater.* **15**, 035013 (2014).
- 36) N. Miki and S. M. Spearing, *J. Appl. Phys.* **94**, 6800 (2003).
- 37) H. Takagi, R. Maeda, T. R. Chung, N. Hosoda, and T. Suga, *Jpn. J. Appl. Phys.* **37**, 4197 (1998).
- 38) S. Hashimoto et al., *Surf. Interface Anal.* **18**, 799 (1992).
- 39) R. A. Khmelnsky and A. A. Gippius, *Phase Transit.* **87**, 175 (2014).
- 40) V. L. Kuznetsov, I. L. Zilberberg, Y. V. Butenko, A. L. Chuvilin, and B. Segall, *J. Appl. Phys.* **86**, 863 (1999).
- 41) S. E. Grillo and J. E. Field, *J. Phys. D: Appl. Phys.* **30**, 202 (1997).
- 42) H. Takagi, Y. Kurashima, A. Takamizawa, T. Ikegami, and S. Yanagimachi, *Jpn. J. Appl. Phys.* **57**, 02BA04 (2018).